ChemComm

COMMUNICATION

View Article Online
View Journal | View Issue

Cite this: *Chem. Commun.*, 2024, **60**, 12245

Received 25th July 2024,
Accepted 20th September 2024

DOI: 10.1039/d4cc03739a

rsc.li/chemcomm

Asymmetric phthalocyanine-based hole-transporting materials: evaluating the role of heterocyclic units and PMMA additive†

Sifa Dogan,[a] Muhittin Unal,[b] Perihan Kubra Demircioglu,[a] Desiré Molina,*[c] Mine Ince*[a] and Seckin Akin*[bd]

Two novel asymmetric phthalocyanine derivatives, ZnPc-1 and ZnPc-2, are synthesized to enhance charge transfer properties and mitigate deep-level traps on the perovskite surface using electron-rich nitrogen atoms. PSCs with ZnPc-1 and ZnPc-2 as hole-transporting materials (HTMs) achieved power conversion efficiencies (PCEs) of 12.11% and 8.98%, respectively. Incorporating a small amount of PMMA into the HTM solution significantly improved performance, resulting in PCEs of 16.2% and 12.5% for ZnPc-1 and ZnPc-2, respectively. The addition of PMMA enhances conductivity and prevents moisture intrusion, boosting both the efficiency and stability of PSCs.

While perovskite solar cells (PSCs) have reached power conversion efficiencies (PCEs) of over 26%, they still lag behind conventional silicon-based cells in practical efficiency and stability.[1] These issues primarily arise from the instability of ABX_3 perovskites since the ionic nature of the halide perovskites and external factors lead to defects like under-coordinated Pb^{2+}, lead clusters, and Pb–I antisite defects, creating deep traps that reduce performance and stability.[2,3] Recent passivation techniques, including the use of Lewis bases and acids, have shown promise in addressing these issues.[4] Electron-rich heteroatoms like nitrogen, oxygen, and sulfur bond effectively with under-coordinated Pb^{2+} ions, improving surface defects.[5,6] Snaith *et al.* demonstrated that treating perovskite films with Lewis bases like thiophene and pyridine reduces non-radiative recombination.[7–9] The charge transport layers, specifically the electron transport layer (ETL) and hole transport layer (HTL), are crucial for device performance and stability. Spiro-OMeTAD is the leading hole-transporting material (HTM) used in high-efficiency PSCs but suffers from complex synthesis, restricted charge mobility, and insufficient perovskite layer coverage.[10–12] Its low electrical properties require hygroscopic additives, which enhance performance but harm long-term stability.[13,14] In response, significant research studies over the last decade have focused on developing more efficient HTMs for PSCs. Among various candidates, phthalocyanine (Pc) derivatives have been particularly noteworthy.[15–17] These planar, 18 π-electron aromatic compounds are known for their expansive π-conjugated system, thermal and chemical stability, and strong absorption features, making them suitable for photovoltaic applications. Their rigid structure promotes strong π–π interactions, facilitating efficient charge carrier pathways, a key feature for electronic devices.[18–21] Consequently, over the past decade, Pc-based HTMs have demonstrated competitive performance, achieving PCEs exceeding 20%. Asymmetrically substituted Pcs are gaining attention for their unique photophysical and electrochemical properties, which enhance directional charge transfer in dye-sensitized solar cells.[22] Sastre-Santos *et al.* achieved a PCE of 14.25% with an asymmetric ZnPc, surpassing the 10.52% efficiency of symmetric ZnPc.[23] Their further research showed that fluorinated asymmetric ZnPc outperformed others, reaching an efficiency of 15.40% due to its higher conductivity.[24] In our previous research, we compared unsymmetrical ZnPc derivatives with three *tert*-butyl and one carboxylic acid groups to their symmetrical counterparts in double-cation mixed PSCs. The asymmetric ZnPc achieved a moderate efficiency of 13.7%. However, the potential passivation effects and interactions with perovskite and carboxylic acid were not fully explored.[25] Based on these results, we developed novel asymmetrically substituted ZnPc derivatives (**ZnPc-1** and **ZnPc-2**) with pyridine and imidazole groups to improve charge transfer efficiency and reduce deep-level traps on the perovskite surface through the passivation effects of electron-rich nitrogen atoms in these heterocyclic units. Furthermore, various concentrations of PMMA were added to the HTM solution. Seok *et al.* reported that using PMMA as an intermediate layer between perovskite and CuPc reduces surface

[a] *Department of Natural and Mathematical Science, Tarsus University, 33400, Tarsus, Turkey. E-mail: mine.ince@tarsus.edu.tr*
[b] *Laboratory of Advanced Materials & Photovoltaics (LAMPs), Necmettin Erbakan University, 42090, Konya, Turkey*
[c] *Area de Química Orgánica, Instituto de Bioingeniería, Universidad Miguel Hernández, 03202, Elche, Spain*
[d] *Department of Metallurgical and Materials Engineering, Necmettin Erbakan University, 42090, Konya, Turkey*

† Electronic supplementary information (ESI) available. See DOI: https://doi.org/10.1039/d4cc03739a

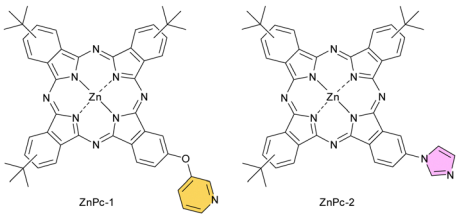

Scheme 1 Chemical structures of **ZnPc-1** and **ZnPc-2**.

defects and prevents electron transport from the perovskite to the CuPc layer, improving efficiency and stability.[26] Our study aims to enhance film formation by incorporating PMMA into the ZnPc-based HTL matrix, resulting in homogeneous and densely packed HTLs that boost both efficiency and stability. Here, we present the molecular engineering of Pc-based HTMs by incorporating imidazole and pyridine as functional groups capable of interacting with the perovskite surface (Scheme 1). The synthesis of ZnPcs 1 and 2 was achieved in a single-step reaction through the cyclotetramerization of 4-*tert* butylphthalonitrile and the corresponding imidazole or pyridyloxy phthalonitrile in the presence of $Zn(OAc)_2$.

Purification *via* silica gel column chromatography yielded **ZnPc-1** and **ZnPc-2** in 50% and 31% yield, respectively. The structures of these new ZnPcs were confirmed through MALDI-TOF MS spectrometry, IR, UV/Vis, and NMR spectroscopies (Fig. S1–S4, ESI†).

Fig. 1a shows the electronic absorption spectra of **ZnPc-1** and **ZnPc-2**, which are similar, with the Soret B band at 350 nm and the Q band at 673 nm. The electrochemical characterization of ZnPcs was conducted using cyclic voltammetry (CV) in dry THF, with ferrocene utilized as an external standard (Fig. S5, ESI†). The highest occupied molecular orbital energy levels (E_{HOMO}) were determined through the equation $E_{HOMO} = E^1_{ox}$ (V) *vs.* Fc/Fc^+, positioning the ferrocene oxidation potential at 0.7 V *vs.* the normal hydrogen electrode (NHE). The lowest unoccupied molecular orbital energy levels (E_{LUMO}) of ZnPcs were calculated by adding the optical bandgap to the E_{HOMO} value.[27] Table S1 (ESI†) shows the optical and electrochemical characteristics of the ZnPc derivatives. Fig. 1b compares the energy levels of perovskite, spiro-OMeTAD, and ZnPc-based HTMs. Assuming that mixed-ion perovskite HOMO/LUMO energy levels are at −5.65 eV/−4.05 eV,[28] all E_{HOMO} values of ZnPcs indicate energetic favorability, implying efficient charge extraction at the interfaces. Fig. 1b delineates the energetic profile of the constituent components within the photovoltaic devices. The cross-sectional scanning electron microscopy (SEM) image reveals the stratified architecture of the devices assembled utilizing **ZnPc-1** as the HTL as an example (Fig. 1c). The experimental design for the photovoltaic studies focused on evaluating the effects of novel HTMs and the incorporation of PMMA into the HTL on device performance. Triple-cation PSCs with the architecture FTO/c-TiO_2/mp-TiO_2/perovskite/HTL/Ag were the subject of these investigations, with devices containing lithium bis(trifluoromethanesulfonyl)imide (Li-TFSI) and 4-*tert*-butylpyridine (*t*BP) doped spiro-OMeTAD utilized as a control point. Initial application of pristine **ZnPc-1** and **ZnPc-2** at a concentration of 20 mg mL^{-1} in chlorobenzene yielded modest device performance, with recorded PCEs of 1.91% and 2.16%, respectively. However, consistent with previous observations for analogous materials, it was anticipated that these outcomes would undergo enhancement over time.[29] Indeed, subsequent measurements taken after a ten-day interval revealed a substantial enhancement, with the PCE for **ZnPc-1** tripling to 5.67% and for **ZnPc-2** doubling to 3.65% (Fig. S6, ESI†). To enhance PSC performance, devices with HTMs doped with Li-TFSI and tBP were fabricated, achieving initial PCEs of 11.75% for **ZnPc-1** and 8.42% for **ZnPc-2**. Over ten days, **ZnPc-1** improved to 12.11% and **ZnPc-2** to 8.98% (Fig. S7, ESI†). Given that doped **ZnPc-1** showed the best performance, it was further tested at chlorobenzene concentrations of 10, 20, and 30 mg mL^{-1}, with 20 mg mL^{-1} being optimal (see Fig. S8 and S9, ESI†). SEM images of the devices at 10 mg mL^{-1} (Fig. S10, ESI†) reveal uncovered perovskite surfaces, explaining the lower PCE at this concentration. Further investigation focused on the potential positive impact of PMMA additions on device functionality. Devices containing 0.5% (PMMA-1×), 1.0% (PMMA-2×), and 1.5% (PMMA-3×) weight/weight of PMMA relative to **ZnPc-1** in the HTM solution were studied. Fig. 2a demonstrates that 1.0% PMMA addition was most beneficial, enhancing efficiency up to 16.2% (J_{sc} (short-circuit current density) = 22.09 mA cm^{-2}, V_{oc} (open-circuit voltage) = 1.05 V and FF (fill factor) = 69.9%) in contrast to 15.3% and 14.7% PCE for PMMA-1× and PMMA-3×, respectively. The boxplots of the photovoltaic parameters revealed that the FF and V_{oc} were the metrics that experienced amelioration (Fig. S11, ESI†). This could be attributable to the insufficiency of 0.5% PMMA in conferring adequate HTL homogeneity, and the adverse impact of 1.5% PMMA on conductivity due to its inherent insulative nature.[30] The findings indicate that balancing PMMA concentration is crucial for achieving both homogeneity and conductivity in the HTL, affecting device performance. With optimal ZnPc/PMMA HTL conditions established, **ZnPc-2** was also tested, reaching a maximum PCE of 12.5% and showing more discrete photovoltaic parameters compared to **ZnPc-1** (see Fig. S12 and S13, ESI†). ZnPc-based devices exhibited lower PCE than that of the spiro-OMeTAD-based control device with an efficiency of 21.1%, a V_{oc} of

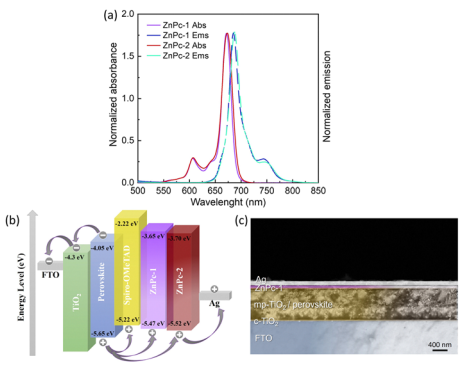

Fig. 1 (a) UV-vis absorption (solid line) and emission (dashed line) spectra of **ZnPc-1** and **ZnPc-2** in THF. (b) Energy level diagram of the devices used in this study. (c) Cross-sectional SEM image of the **ZnPc-1** HTL employing a device with a concentration of 20 mg mL^{-1}.

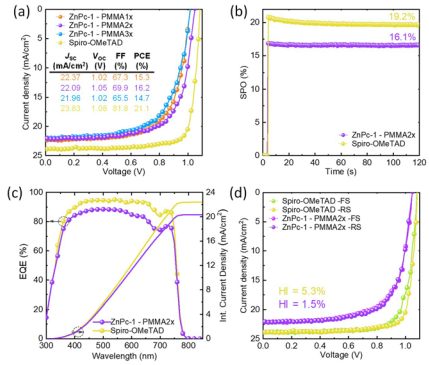

Fig. 2 (a) The J–V curves of the best-performing spiro-OMeTAD-based control device and **ZnPc-1** (20 mg mL^{-1}) devices fabricated with different PMMA concentrations. (b) SPO curves, (c) EQE curves, and (d) hysteresis curves of the best-performing devices.

1.08 V, a J_{sc} of 23.83 mA cm^{-2}, and an FF of 81.8%. Despite exhibiting a lower PCE compared to spiro-OMeTAD (16.1% *vs.* 19.2%), the stability profile depicted in the stabilized power output (SPO) graph indicates that **ZnPc-1**/PMMA-2× attains stability more rapidly and maintains it consistently over time (Fig. 2b), referring a stable conductivity over time due to good interfacial contact. External quantum efficiency (EQE) curves reveal that while the EQE of the **ZnPc-1**/PMMA-2× device does not eclipse that of the control device, it displayed a congruent trajectory with spiro-OMeTAD, corroborated by the integrated current density that aligns with the photovoltaic data (Fig. 2c). Reverse and forward scan assessments of **ZnPc-1**/PMMA-2× devices indicated a negligible hysteresis index (HI = 1.5%) compared to spiro-OMeTAD-based devices (HI = 5.3%) (Fig. 2d). The reduction in HI is due to efficient charge injection at the perovskite/HTM interface, preventing hole accumulation at the HTL/perovskite interface, as confirmed by conductivity results. The obtained curves demonstrate that before PMMA doping, the HTL matrix lacks continuity, resulting in lower conductivity (Fig. S14, ESI†). Conductivity measurements in PMMA-employing devices revealed a larger current on the structure with the **ZnPc-1** HTM, showing more excellent conductivity. Additionally, the presence of pyridine and imidazole groups contributes to the high-quality perovskite film, leading to the elimination of surface defects. The combined effects result in improved charge transport and reduced hysteresis, highlighting the significance of interface engineering and surface modification for enhanced device performance in PSCs. To confirm the universality of PMMA doping, devices using spiro-OMeTAD with PMMA additives were tested (Fig. S15, ESI†). The results show that PMMA doping enhances the photovoltaic parameters of spiro-OMeTAD-based devices. In comparison to the control device shown in Fig. 2a, the champion device using PMMA-doped spiro-OMeTAD showed a PCE of 22.0% with a V_{oc} of 1.13 V, a J_{sc} of 23.74 mA cm^{-2}, and an FF of 82.1% with acceptable reproducibility.

Fig. S16 (ESI†) shows the SEM and AFM images of the engineered surfaces. The ZnPc-PMMA-2× mixtures achieved optimal coverage with no pinholes (Fig. S16b and c, ESI†), whereas the spiro-OMeTAD-based control film showed imperfections (Fig. S16a, ESI†). Surface roughness is crucial for device performance; a smoother HTL surface reduces charge recombination and improves efficiency and stability. Fig. S16e (ESI†) demonstrates that the **ZnPc-1**/PMMA-2× film has a more planar surface with a roughness of 9.6 nm, compared to **ZnPc-2**/PMMA-2×, which has a more corrugated morphology with 15.3 nm roughness. The higher roughness in ZnPc HTMs arises from the thinner film on the perovskite layer, leading to incomplete surface coverage and reduced surface planarization. Furthermore, the Pc layers without PMMA are almost imperceptible, highlighting the crucial role of PMMA in promoting a discernible and substantial film (Fig. S17, ESI†). Compared to the bare perovskite surface, all HTL films reduce surface roughness, creating a smoother perovskite interface and enhancing device performance (Fig. S18, ESI†). To examine hole-transport properties at the HTL/perovskite interface, steady-state (PL) and time-resolved photoluminescence (TRPL) measurements were performed (Fig. S19, ESI†). The results show notable PL quenching of about 98%, 97%, and 94% for perovskite films with spiro-OMeTAD, **ZnPc-1**, and **ZnPc-2** HTLs, respectively, compared to the HTL-free film. This quenching indicates that the HTL effectively facilitates charge transfer, thereby reducing the PL intensity. Examining Fig. S19c and d (ESI†), it is evident that **ZnPc-1** (94.7 ns) exhibits a shorter average decay time than that of **ZnPc-2** HTM (99.0 ns), and this effect is comparable to that of the control film (80.1 ns). The acquired findings have been summarized in Table S2 (ESI†). Given that increased PL quenching reflects enhanced hole extraction along the perovskite/HTL interface, these findings suggest that **ZnPc-1** HTL demonstrates superior hole-extraction efficiency compared to the **ZnPc-2** HTL. We also investigated the chemical interaction of the perovskite/HTM interfaces, assessing their defect passivation function using XPS (Fig. S20, ESI†). In Fig. S19e and f (ESI†), the binding energies of the primary peaks, Pb $4f_{7/2}$ and Pb $4f_{5/2}$, for the control film are 138.3 and 143.1 eV, respectively. Surface passivation treatment causes a noticeable shift towards higher energy values for both peaks in the perovskite films. Specifically, Pb $4f_{7/2}$ and Pb $4f_{5/2}$ peaks for **ZnPc-1** and **ZnPc-2**-passivated films shift to (138.6/143.4 eV) and (138.4/143.2 eV), respectively, 0.3 eV and 0.1 eV higher than those of the control film. This shift confirms the interaction between the passivation agents and under-coordinated Pb^{2+}. Notably, **ZnPc-1** shows a more pronounced shift than **ZnPc-2**, suggesting stronger interaction with under-coordinated Pb^{2+}. Additionally, the I 3d peaks exhibit a similar trend after **ZnPc-1** and **ZnPc-2** deposition, consistent with findings reported by Huang *et al.*[31] Furthermore, long-term stability studies of the ZnPc/PMMA-2× devices were carried out comparing them with control devices. The progression of the different photovoltaic parameters in ambient conditions was studied, called the shelf stability test, with relative humidity adjusted to 40 ± 10% under light soaking. Fig. S21a (ESI†) illustrates that the **ZnPc-1**/PMMA-2× device retains over 80% of its initial PCE after nearly 900 hours, whereas the **ZnPc-2**/PMMA-2× devices show a decrease of more than 30% in

original PCE. In contrast, the control device drops below 40% PCE after 500 hours (Fig. S22, ESI†). Moreover, following a thermal stress test at 85 °C for 48 hours, SEM imaging (Fig. S23, ESI†) reveals no significant changes in the **ZnPc-1**/PMMA-2× films. However, a notable decline in PCE is observed, with a 20% reduction within the first 24 hours and exceeding a 60% decrease for spiro-OMeTAD devices (Fig. S24, ESI†). This decline is likely attributed to Ag penetration from the electrode, altering the HTL, including the formation of trap states and changes in energy barriers at the perovskite/HTL interface.[32,33] The hydrophobic nature of the HTL was shown by measuring the contact angles of deionized water droplets on HTL films (Fig. S21b–d, ESI†). The contact angle obtained for **ZnPc-1**/PMMA-2× was 92.5°, while that for the **ZnPc-2** counterpart was 85.9°. In contrast, the control film displayed a considerably lower contact angle of 53.7°, even surpassing the angle measured for the **ZnPc-1** film without PMMA, which registered at 88.7° (Fig. S25, ESI†). A higher contact angle suggests that humidity penetration in perovskite devices is reduced, thereby improving their long-term stability. These results also indicate that the addition of PMMA has minimal effect on the films' hydrophobicity, as evidenced by consistently similar contact angles across various configurations. To better understand the differences in stability between **ZnPc-1**/PMMA-2× and spiro-OMeTAD, the response of the devices was measured for 60 seconds, subjecting them to periods of five seconds of illumination interspersed with periods of 5 seconds in darkness (Fig. S26a and b, ESI†). The device incorporating **ZnPc-1**/PMMA-2× as the HTL exhibited remarkable resilience, recovering nearly full operability in each successive cycle, in contrast to the control device which demonstrated a progressive loss of functionality with each cycle. The V_{OC} decay time of the **ZnPc-1**/PMMA-2× devices was much more progressive than that of the control devices, which decayed almost when irradiation stopped, which may indicate a better quality of the interface and agrees with the results of stability studies (Fig. S26c, ESI†).

In summary, two asymmetric ZnPcs with functional groups capable of interacting with the perovskite layer have been designed and synthesized. These new derivatives have been studied as HTMs for PSCs in the n–i–p configuration. The maximum efficiencies of 12.11% and 8.98% were obtained with **ZnPc-1** and **ZnPc-2** derivatives, respectively. Adding 1% PMMA to the HTM precursor solution significantly improved the performance, boosting the PCEs to 16.2% for **ZnPc-1** and 12.5% for **ZnPc-2**. The ZnPc/PMMA-based HTLs provided the PSC devices with higher stability than that achieved with spiro-OMeTAD. Although this hypothesis warrants additional investigation, the enhancement could be attributed to the increased homogeneity of the HTL when PMMA is incorporated, coupled with the improved interfacial contact characterized by a reduced presence of defects. Therefore, this approach not only reduces costs and simplifies the processing, but also opens a new field of study that could extend to other layers of the devices and to other materials currently employed as interlayers.

S. D., P. K. D. and M. I performed the synthesis and characterization of Pcs. M. U., S. A., and D. M., fabricated the PSCs, and conducted characterizations. M. I., S. A., and D. M., prepared the manuscript. All the authors contributed to the analysis of the results and manuscript revision.

This work has been supported by The Scientific and Technological Research Council of Turkey, TUBITAK (Grant: 123F145).

Data availability

The data supporting this article have been included as part of the ESI.†

Conflicts of interest

There are no conflicts to declare.

Notes and references

1 J. Jeong, *et al.*, *Nature*, 2021, **592**, 381–385.
2 J. Siekmann, *et al.*, *Adv. Energy Mater.*, 2023, **13**, 2300448.
3 S. Akin, *et al.*, *Adv. Energy Mater.*, 2020, **10**, 1903090.
4 L. Fu, *et al.*, *Energy Environ. Sci.*, 2020, **13**, 4017–4056.
5 Y. Yang, *et al.*, *J. Chem. Eng.*, 2023, **451**, 138962.
6 L. Yu, *et al.*, *J. Chem. Eng.*, 2021, **420**, 129931.
7 X. Zhao, *et al.*, *ACS Appl. Energy Mater.*, 2021, **4**, 6903–6911.
8 A. Semerci, *et al.*, *Adv. Opt. Mater.*, 2023, **11**, 2300267.
9 B. Chen, *et al.*, *Chem. Soc. Rev.*, 2019, **48**, 3842–3867.
10 J. Y. Seo, *et al.*, *Energy Environ. Sci.*, 2018, **11**, 2985–2992.
11 Y. Liu, *et al.*, *Angew. Chem., Int. Ed.*, 2020, **59**, 15688–15694.
12 N. Arora, *et al.*, *Small*, 2019, **15**, 1904746.
13 S. Akin, *et al.*, *Adv. Funct. Mater.*, 2022, **32**, 2205729.
14 H. S. Kim, *et al.*, *Nano Energy*, 2019, **61**, 126–131.
15 M. Pegu, *et al.*, *J. Mater. Chem. C*, 2020, **10**, 11975–11982.
16 D. Molina, *et al.*, *J. Mater. Chem. C*, 2023, **11**, 7885–7919.
17 J. Zhang, *et al.*, *J. Chem. Eng.*, 2023, **459**, 141573.
18 M. Urbani, *et al.*, *Coord. Chem. Rev.*, 2019, **381**, 1–64.
19 D. Molina, *et al.*, *J. Porphyr. Phthalocyanines*, 2019, **23**, 546–553.
20 Y. Matsuo, *et al.*, *RSC Adv.*, 2020, **10**, 32678–32689.
21 D. Gounden, *et al.*, *Coord. Chem. Rev.*, 2020, **420**, 213359.
22 M. Ragoussi, *et al.*, *Eur. J. Org. Chem.*, 2013, 6475–6489.
23 P. Huang, *et al.*, *ACS Appl. Energy Mater.*, 2021, **4**, 10124–10135.
24 A. Hernández, *et al.*, *J. Mater. Chem. C*, 2023, **11**, 8243–8253.
25 Y. Zhang, *et al.*, *ACS Appl. Energy Mater.*, 2018, **1**, 2399–2404.
26 H. Kim, *et al.*, *Adv. Funct. Mater.*, 2022, **32**, 2110473.
27 K. T. Cho, *et al.*, *Adv. Energy Mater.*, 2017, **7**, 1601733.
28 S. Mabrouk, *et al.*, *J. Mater. Chem. A*, 2018, **6**, 7950–7958.
29 D. Molina, *et al.*, *ChemPhotoChem*, 2020, **4**, 307–314.
30 U. Ali, *et al.*, *Polym. Rev.*, 2015, **55**, 678–705.
31 K. Zou, *et al.*, *ACS Mater. Lett.*, 2022, **4**, 1101–1111.
32 J. Li, *et al.*, *Adv. Energy Mater.*, 2017, **7**, 1602922.
33 J. Zhuang, *et al.*, *Nano-Micro Lett.*, 2023, **15**, 84.

